Chapter 4
Optimal Pulse Shaping for Ultrafast Laser Interaction with Quantum Systems

Hyosub Kim, Hangyeol Lee, Jongseok Lim and Jaewook Ahn

Abstract Coherent control method steers a quantum system to a desirable final quantum state among a number of final states otherwise possible in a given light-matter interaction, by using a specially shaped light form programmed in its spectral and/or temporal domain. In this chapter, we briefly review a number of light-form shaping methods previously considered for coherent control of ultra-fast laser interaction with atoms, and provide their application examples along with their experimental demonstrations.

4.1 Introduction

Latest development in laser optics manifests a new capability of light, other than the traditional use of light as a viewing tool, which is the use of light as a control tool. In particular, along with the advent of ultra-fast optical techniques, it becomes possible that the versatile light forms are newly engineered by programming the amplitude and shape functions of the broad frequency range of an ultra-fast optical pulse. As a result, the programmed spectral and/or temporal shape of a laser pulse can be used as a quantum-mechanical means to control the dynamics of a quantum system. This field of optical research is refereed to as coherent control, or quantum control, or more specifically to emphasize the usage of ultra-fast laser, "ultra-fast quantum control."

Examples of the coherent control concepts demonstrated in terms of shaped light-matter interactions can be found in numerous experiments. To list a few, historically Wilson and coworkers [1] experimentally realized closed-loop feedback control of optimal pulse shape for efficient population transfer in molecular system. Gerber

H. Kim · H. Lee · J. Lim · J. Ahn (✉)
Department of Physics, Korea Advanced Institute of Science and Technology (KAIST),
291 Daehak-ro, Yuseong-gu, Daejeon 305-701, Korea
e-mail: jwahn@kaist.ac.kr

K. Yamanouchi et al. (eds.), *Progress in Ultrafast Intense Laser Science XI*,
Springer Series in Chemical Physics 109, DOI: 10.1007/978-3-319-06731-5_4,

and coworkers [2] also demonstrated the coherent control in the photo-dissociation process of molecules, by using shaped ultra-fast optical pulses which were adaptively programmed in a closed control loop consisted of a laser programming apparatus and a photo-fragment mass spectroscope. Although the adaptive control methods are powerful in many real applications, we leave this class of coherent control methods aside and focus on the open-loop coherent control method, where the laser pulse shape is first designed by solving the Schrödinger equation for the given light-matter interaction. In that context, Silberberg and coworkers [3] initiated the pulse shape design research in terms of coherent control in their demonstration of atomic nonlinear absorption process. Other examples can be found, for example, in optical second-harmonic generation [4], optical third-harmonic generation [5], multi-photon absorption [6, 7], and coherent anti-Stokes Raman scattering [8]. More advanced applications can be found in in-vivo fluorescence microscopy [9], coherent control quantum bits in Rydberg atoms [10], and semiconductor [11] to list a few.

The research of coherent control of quantum dynamics has become possible in many ways thanks to the development of laser pulse shaping apparatus in the last two decades [12]. Among many apparatus, spatial light modulators (SLM), in particular, allow a relative easy way to engineer the interference among the transition pathways of a multi-photon absorption process, because of their Fourier domain spectral shaping capability [3, 6]. Also, acousto-optic programmable dispersive filters (AOPDF) provide more sophisticated ways of pulse-shaping in the context of this chapter, showing its capability, for example, in the strong-field multi-photon absorption control of alkali atoms [7, 13]. A combination of those pulse-shaping devices can transform a well-defined gaussian-shape pulse to an arbitrary pulse shape of programmed spectral phase, amplitude, and also polarization [14–18].

4.2 Types of Pulse Shaping

Before we begin to describe the coherent control experiments, we categorize the ways of pulse shaping methods. To do that, we first need to define an ultra-fast laser pulse.

The ultra-fast laser pulse can be represented either in time domain as $E(t)$, or in frequency domain $\tilde{E}(\omega)$, where their mutual relation is given by the complex Fourier transform ($\mathscr{F}$). The most interesting case in this context of ultra-fast optical pulse shaping is a moderately short pulse, which means the center carrier frequency ω_0, and the bandwidth of the pulse $\Delta\omega$ are related as $\Delta\omega \ll \omega_0$ [19]. Then, without a loss of generality, the electric field is factored into the envelope and carrier functions given by

$$E(t) = \frac{1}{2}\varepsilon(t)e^{i\phi(t)}e^{i\omega_0 t} + c.c., \tag{4.1}$$

and its frequency domain representation is given by

$$\tilde{E}(\omega) = \mathscr{F}\{E(t)\} = |\tilde{E}(\omega)|e^{i\Phi(\omega)}, \tag{4.2}$$

where the tilde denotes a complex value and, since $E(t)$ is real function, a relation $\tilde{E}(\omega) = \tilde{E}^*(-\omega)$ holds.

It is noted that we neglect the spatial profile of the laser pulse, which often plays an important role in nonlinear optical process in terms of spatial average effect [20], but we assume the given light-matter interaction is performed in an uniform spatial intensity region only.

As seen in (4.1), the electric field of the pulse is described by its center carrier frequency ω_0 and its transient envelope function $\varepsilon(t)$. The Fourier transform of this temporal profile yields the same analogy in the frequency domain, which is centered at ω_0. Here, we call $|\tilde{E}(\omega)|$ as a spectral amplitude and $\Phi(\omega - \omega_0)$ as a spectral phase. It is noted that the spectral phase is a function of frequency, and, in particular, if the spectral phase is a constant over the whole spectrum range, the laser pulse is referred to as a Fourier transform-limited pulse.

The spectral phase can be expanded into a Taylor series as

$$\Phi(\omega) = \Phi(\omega_0) + \Phi'(\omega - \omega_0) + \frac{1}{2}\Phi''(\omega - \omega_0)^2 + \frac{1}{6}\Phi'''(\omega - \omega_0)^3 + \cdots, \tag{4.3}$$

where the constant phase $\Phi(\omega_0)$ is the carrier-envelop phase, Φ' is the movement of pulse envelope along the positive time direction, (which is in fact equivalent to the frequency shift of ω_0), Φ'' is the linear spectral chirp, and Φ''' is the quadratic spectral chirp, etc. As a pulse shape contains both the envelop shape and phase information at the same time, pulse shaping control is equivalent to both the amplitude and phase shape manipulation of the laser pulse. Also, as the actually time and frequency domains are related with respect to the Fourier transform relation, only one of the domain control, either time or frequency, is sufficient for the generation of a desired shape programming of a laser pulse.

The pulse shaping device generally operates in spectral domain, to be discussed in Sect. 4.3, so we can categorize the types of pulse shaping in spectral domain as following:

1. Amplitude shaping (lose photons: irreversible shaping)
   a. Spectral amplitude blocking
   b. Wavelength scanning (regular spectroscopy)
2. Phase shaping (temporal rearrangement of spectral components)
   a. Spectral chirping
   b. Multiple pulses (e.g., 2D-Fourier transform spectroscopy)
   c. Spectral phase gating
   d. Spectral phase step

The amplitude shaping methods in spectral domain inevitably lose photons, and, therefore, this type of pulse shaping methods is intrinsically an irreversible process. However, to be described in Sect. 4.4, certain light-matter interactions are better performed with a smaller set of spectral components of light. For example, in the two-photon absorption case in a three-level atom with an intermediate energy level, a certain part of laser spectrum participates to the net absorption as a destructive quantum interference. Therefore, removing those spectral components, to make the remaining absorption pathways all constructively interfere with each other, could enhance the net absorption probability. This method is known as spectral blocking [6, 21, 22]. Another method is a wavelength scanning which could be implemented by allowing only a narrow spectral region of an ultra-fast pulse and blocking the others.

The spectral phase shaping is a way of temporal rearrangement of spectral components, and this method allows a variety of ways of spectral manipulation of a laser pulse. For example, spectral phase gating method provides a narrow spectral window region (phase-gated window) to be of different phase from the others, and scans the phase-gated spectral window from one end to the other end of the laser spectrum. Also, one can make a spectral phase step in a certain spectral location of the spectrum and scan the phase-step location, or one can implement a modulated spectral phase function $\Phi(\omega) = A\cos(B\omega + C)$ and by controlling the modulation amplitude A, the modulation frequency B, or the modulation phase C, respectively, the population transfer among the energy levels of the given light-matter interaction can be enhanced or suppressed. Another example is a use of multiple laser pulses, which can be programmed in the phase-shaping in spectral domain. For example, a set of three laser pulses with a fixed carrier-envelope phase and variable time delays implements two-dimensional Fourier transform spectroscopy. One could change the frequency de-tuning, the spectral linear chirp, or the spectral quadratic chirp by changing Φ', Φ'', or Φ''', respectively, which subject will be discussed in more detail in Sect. 4.5. Lastly, if the transition phase information is completely known a priori, then a spectral phase function which maximizes the given transition can be programmed to be discussed in Sect. 4.6.

4.3 Pulse Shaping Devices

Although the pulse shaping methods are performed in both the Fourier and time domains, the tailored pulse can be described in either domain completely. Thus we concentrate on the frequency domain[1] shaping here. When we deal with a pulse at frequency domain, angular dispersive optical elements, such as a prism or a diffraction grating, can be used [23, 24]. As such optical elements disperse each chromatic component at a different spatial position in the real plane, managing each chromatic

[1] We notice that Fourier domain and frequency domain have the same physical meaning in this chapter.

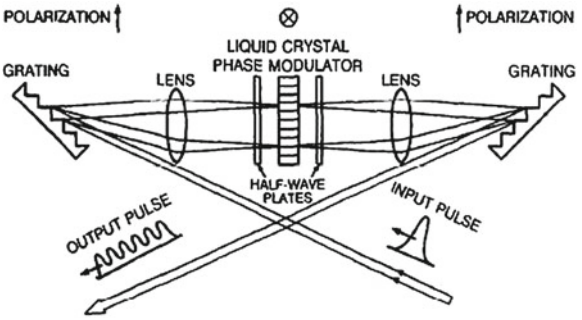

Fig. 4.1 An optical pulse shaper combined with a pair of diffraction gratings and a liquid crystal SLM. Phase, and amplitude, or both phase and amplitude are controllable according to respective types of configurations of an SLM, inserted wave plates, and polarizers. The image is from [27] with permission by the publisher

ray at different position would possibly manipulate the shape of the pulse in the frequency domain. In the contrary to frequency domain, time domain control can be done by acousto-optic effect [16]. Programmable acoustic waves generated by piezo-electric transducer in an acousto-optic crystal convolute with incident pulses and generate desired pulse shape.

Spectral amplitude and phase functions can be controlled either by a fixed mask [23], or by a variable masks: For example, SLM [25, 26], AOPDF [17], and etc [27]. We briefly describe the working principles of SLM and AOPDF, before we start to discuss the experiments performed with these devices.

4.3.1 Spatial Light Modulator

SLM is an array of optical phase or amplitude (or both) modulators made out of liquid crystals. The liquid crystal in a nematic phase is a uniaxial birefringent material and its molecular orientation is easily controllable by means of an applied electric field. A usual setup, shown in the Fig. 4.1, is used as an optical pulse shaper, where an SLM pulse shaper is located in the Fourier plane of a 2f-to-2f configuration of lens and diffraction grating setup, also known as Martinez zero-dispersion stretcher setup [27, 28]. The phase of light transmitted through each liquid crystal pixel is given as a function of both the incident polarization and the electric field applied to the pixel. For example, in the case of a phase-only modulation SLM, the extra-ordinary axis of the liquid crystal is oriented originally parallel to incident polarization and, when the electric field is applied to the propagating direction of light, optical path length can be managed without birefringence. With appropriate combinations of half-wave plates and polarizers, amplitude-modulation and both amplitude-and-phase modulation are also possible.

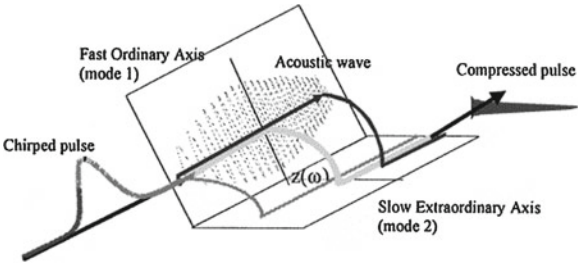

Fig. 4.2 Schematic of the AOPDF. Traveling acoustic wave diffracts phase-matched optical mode. The image is from [17] with permission by the publisher

4.3.2 Acousto-Optic Programmable Dispersive Filter

The working principle of AOPDF is based on collinear acousto-optic interaction, where a programmed acoustic wave diffracts different spectral components, of an ultra-fast laser pulse, that are respectively phase-matched with different acoustic modes in the AOPDF [16]. Thus, the output laser spectral amplitude E_{out} is programmed as $E_{\text{out}} \propto E_{\text{in}} S(\alpha\omega)$, where E_{in} is the input laser spectral amplitude and $S(\alpha\omega)$ is the acoustic mode amplitude and α is the ratio between the speed of sound and the speed of light in the crystal (Fig. 4.2).

4.4 Spectral Amplitude Blocking

4.4.1 A Ladder-Type System

As the first example of coherent control experiments, we consider the spectral blocking among spectral amplitude shaping methods. The quantum system under consideration is the three-level system in a ladder configuration of atomic rubidium (Rb). The three energy levels are the 5S (the ground state), $5P_{1/2}$ (the intermediate state), and 5D states (the final state), as shown in the Fig. 4.3. The coherent light source is from a mode-locked Ti:sapphire laser, of which the wavelength center is at 778 nm and the broad wavelength width of 18 nm in FWHM (the full width at half maximum) covers both the upper and lower intermediate states energy separation.

The transition probability amplitude to the final state is given by the second order time dependent perturbation theory [6] as,

$$c^{(2)}(t) = -\frac{1}{\hbar^2} \sum_i \mu_{fi}\mu_{ig} \int_{-\infty}^{t} \int_{-\infty}^{t_1} E(t_1)E(t_2)e^{i\omega_{fi}t_1} e^{i\omega_{ig}t_2} dt_2 dt_1, \tag{4.4}$$

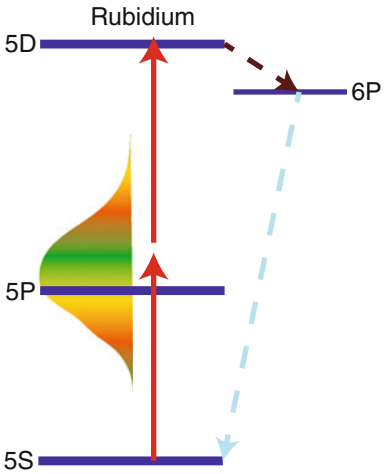

Fig. 4.3 Energy level diagram of the ladder-type two-photon absorption

where μ_{fi} and μ_{ig} are the transition dipole moments. The angular frequency is defined as energy spacing between the two levels as $\omega_{ij} \equiv (E_i - E_j)/\hbar$. We consider an electric field $E(t)$ given as a pulse as,

$$E(t) = \frac{1}{\sqrt{2\pi}} \int_{-\infty}^{\infty} \tilde{E}(\omega) e^{-i\omega t} d\omega. \tag{4.5}$$

Now, the both $E(t_1)$ and $E(t_2)$ are substituted into (4.4) and the complex integral is conducted with an assumption that fast transient is neglected, or the integration time t is large enough compared to the pulse duration. When the spectral bandwidth covers both the transitions ω_{fi} and ω_{ig}, respectively, from the ground state to the intermediate state and from the intermediate state to the final state, the solution is given by

$$c_{fg}^{(2)} = -\frac{1}{i\hbar^2} \mu_{fi}\mu_{ig} [i\pi \tilde{E}(\omega_{ig}) \tilde{E}(\omega_{fg} - \omega_{ig}) + \mathscr{P} \int_{-\infty}^{\infty} \frac{\tilde{E}(\omega)\tilde{E}(\omega_{fg} - \omega)}{\omega_{ig} - \omega} d\omega], \tag{4.6}$$

where the first term corresponds to the resonant two-photon transition and the second term, the Cauchy integral term, exhibits the broad non-resonant behavior of the two-photon absorption. Such a broad spectral response is originated from the short temporal mediation of the intermediate state and thus a large uncertainty in energy occurs [6], but, as the excited state has a rather long lifetime, the total energy of two photons is conserved. It is noted that the transition probability amplitude of the resonant and non-resonant components have different phase. Especially the constituent

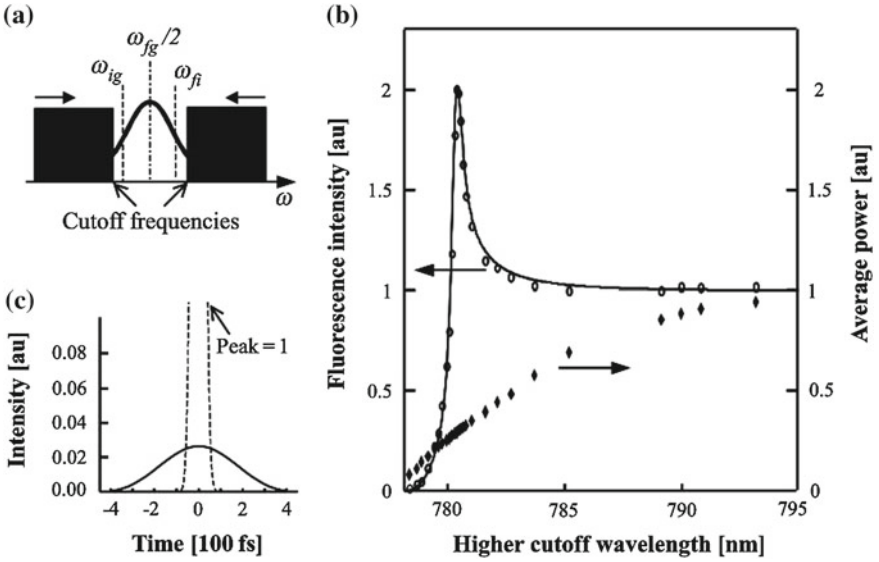

Fig. 4.4 **a** A movable slit blocks the spectral wings. **b** Two photon absorption fluorescence signal with respect to the cutoff wavelength and the corresponding average power. **c** Comparison between the transform limit pulse and the optimized two-photon absorption pulse. The image is from [6] with permission by the publisher

contributions in the non-resonant term destructively interfere within themselves. Therefore, definitely, a transform-limit pulse is not optimal for the given two-photon absorption. Figure 4.4 shows experimental demonstration that the spectral amplitude blocking of the spectral component dramatically increases transition probability amplitude while the pulse energy significantly decreases. In the described experiment, the spectral blocking experiment was carried out by a mechanical slit in the Fourier domain.

4.4.2 Spectral Amplitude Blocking in a V-Type System

The spectral blocking method can be also used for a V-type three level system. To summarize the working principle, the experimental example is explained below.

As shown in Fig. 4.5, the system under consideration is the three energy levels of atomic rubidium, $|g\rangle = 5S$, $|a\rangle = 5P_{1/2}$, and $|b\rangle = 5P_{3/2}$. The two fine structure levels $|a\rangle$ and $|b\rangle$ are simultaneously excited by an ultra-fast laser pulse from the common ground state $|g\rangle$ [21]. The particular transition that we try to control is the two-photon transition from $|a\rangle$ to $|b\rangle$ via $|g\rangle$, the V-type two-photon transition. The corresponding transition probability amplitude can be calculated in a similar manner to the ladder type case, and the resulting formula as a result of the second

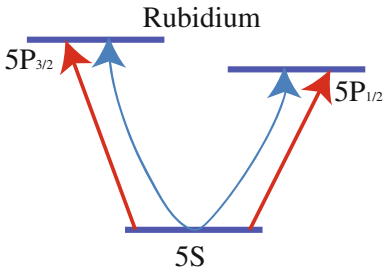

Fig. 4.5 The V-type system of Rb atom. Two-adjacent levels are forbidden transitions

order time dependent perturbation calculation is given by [22],

$$c_{ba}^{(2)} = \frac{1}{i\hbar^2}\mu_{ga}\mu_{gb}[-i\pi\tilde{E}^*(\omega_{ag})\tilde{E}(\omega_{bg}) + \mathscr{P}\int_{-\infty}^{\infty}\frac{\tilde{E}^*(\omega)\tilde{E}(\omega_{ba}+\omega)}{\omega_{ag}-\omega}d\omega], \quad (4.7)$$

where it is noted that the one electric field is the conjugate pair compared to the result in (4.6) of which the feature is originated from the down and upward sequence of the participating three energy states transition.

The experimental observation of the V-type transition to $|b\rangle$ from $|a\rangle$ via $|g\rangle$, which is carried out by detecting the population of $|b\rangle$, needs to be differentiated from the simple one photon transition to $|b\rangle$ from $|g\rangle$. Therefore, the experiments were performed by using a two-dimension Fourier transform spectroscopy technique. By using three optical pulses (the initial preparation pulse, the control pulse, and the final interference pulse, respectively) with different phase oscillation between each states. At the same time, the control pulse was spectrally shaped to implement the spectral blocking for the V-type transition by using AOPDF.

Figure 4.6 shows the experimental results of the enhancement of the two-photon absorption in the V-type system. As evident from the result, the shaped pulse, which has lesser energy than a transform-limited pulse, demonstrates the enhancement of the two-photon transition probability amplitude in the given atomic systems. This results contradicts our intuition that the given non-linear transition is maximized by a transform-limited pulse, which has the maximal peak intensity. However, as the theoretical formula predicts, the given broad-band two-photon transition should be enhanced by eliminating the destructive interference contributions. In the same line of thought, then one could come up with a more efficient way to increase the transition not only by eliminating the destructive interference contributions but by controlling them to constructively interfere with the rest of the transition components, in particular by spectral phase shaping, to be explained in Sect. 4.6.1

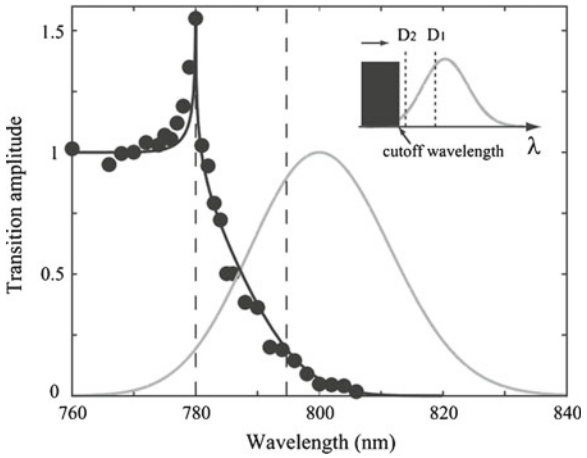

Fig. 4.6 $5P_{1/2}$-$5P_{3/2}$ two-photon transition probability amplitude controlled by the spectral amplitude blocking method. *Dots* represent the experimental measurement and the *dark line* the theoretical calculation. The *grey line* shows the spectrum of the laser pulse. Inset shows the way how the spectrum is blocked. The image is from [21] with permission by the publisher

4.5 Spectral Chirp Control

Chirping is also a crucial parameter for manipulating coherent population control in atom-light interaction. Chirping and quadratic chirping in the frequency domain are described in (4.3) as a Taylor expansion of spectral phase near the center frequency. However, the physical meaning of the linear chirp, or linear spectral chirp, is rather simply understood at the time domain; the oscillating period ω_0 changes as a time dependent variable as $\omega_0 + \beta t$, where the chirp parameter is defined by $\beta = 2\Phi''/(\tau_0^4 + 4\Phi''^2)$ with the time duration τ_0 defined for a corresponding transform-limited pulse (field).[2]

4.5.1 Chirps in a $2 + 1$ *Photon Transition*

The first example of chirp-control experiment is the $2 + 1$ photon transition in an asymmetric three-level ladder system of atomic sodium as shown in Fig. 4.7 [7]. The three-level energy ladder is consisted of the 3S, 4S, and 7P energy states, and the first 3S–4S transition is a two-photon transition, and the second 4S–7P transition is a one-photon transition.

The laser pulses from the femto-second laser amplifier operating at a repetition rate of 1 kHz have the transform-limited pulse duration of 37 fs. Within the allowed

[2] (field) means that the description is about electric field. Readers should care whether (field) or (intensity) arise at the end of a description.

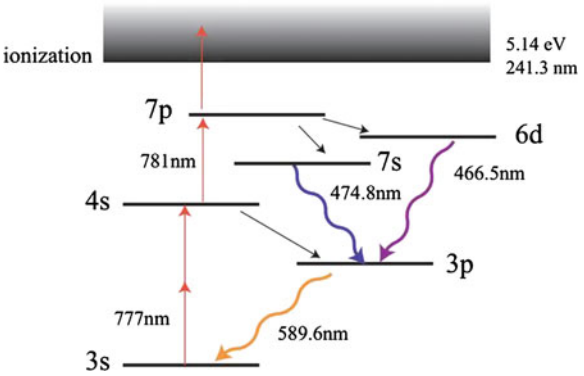

Fig. 4.7 The asymmetric three-level energy ladder in atomic sodium and the 2+ photon transition pathway from 3S to 7P via 4S. The direct four-photon ionized atom signal is 1,000 times smaller than the 4S-7P sequential 2 + 1 photon transition, thus the system is valid as a closed three-level system. The image is from [7] with permission by the publisher

laser bandwidth there is no intermediate state during the two-photon 3S–4S transition, and, therefore, the 3S–4S transition is non-resonant.

When the chirp rate was controlled by AOPDF, as in Fig. 4.8, the 7P state population was measured as a function of the chirp rate of the excitation laser pulse. The experimental results show highly asymmetric behavior of the three photon excited state population given as a function of the chirp rate. The physical origin of the asymmetry can be explained by the different excitation pathways: One is the 4S-state mediated sequential 2 + 1 photon excitation path and the other is a direct three photon excitation path. In the case of the former path, the first two-photon excitation has a higher frequency (777 nm) and the last one-photon excitation has a lower frequency (781 nm), thus the transient character of the excitation process prefers a negative chirp rate and, therefore, is the main reason of the observed asymmetry. The latter path has no reason to have such an asymmetry, rather it shows symmetric behavior with zero population at zero chirp rate, which can be easily observed in the green dot-dashed line in Fig. 4.8. The reason can be understood based on the effect of the dynamic Stark shift which makes the intensity proportional resonance level de-tuning in the presence of the laser pulse [29]. In this scenario, the zero chirp point has the highest intensity, because the largest dynamic Stark shift occurs, and the direct three photon transition path becomes far off de-tuned from the resonance energy condition, which explains the symmetric nature of the intensity shape with a dip at the zero chirp region. Interference between direct path and sequential path causes also considerable effect in multi-photon transition system [30]. However, in the 2 + 1 photon system, calculation based on perturbation theory shows that chirp rates in the experiment are not enough to observe interference fringes.

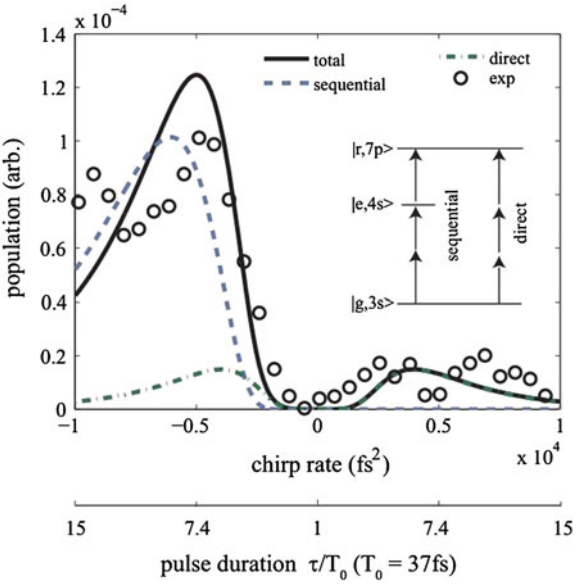

Fig. 4.8 Sodium 2 + 1 photon transition measured as a function of the chirp rate. Experimental results plotted by dots are compared with the theoretical calculation (*the lines*). The 2 + 1, photon sequential transition pathway is in the *blue dashed line* and the three photon direct transition is in the *green dot-dashed line* which are asymmetric and symmetric respectively. The *black solid line* represents the total absorption rate. The image is from [7] with permission by the publisher

4.5.2 Chirps in Two-Photon Transitions

The excitation suppression due to the dynamic Stark effect can be better identified by observing the 3S−4S two-photon transition. As shown in Fig. 4.9, 3S–4S two-photon direct transition path is dominant compared to the four-photon sequential transition path,[3] and, therefore, an observation of the 4s state population as a function of the chirp rate provides a clear evidence for the dynamic Stark effect induced transition reduction.

Experimental result in atomic cesium also finds a similar effect. As a two-photon transition without any resonant intermediate transition, which often referred to as a non-resonant two-photon transition, the 6S–8S transition in cesium is strongly influenced by the dynamic Stark shift in the presence of an intense laser field. In the experiment carried out with a laser intensity around 10^{12} W/cm^2, or in the strong field regime, the chirp rate dependence on the two-photon transition has been investigated [13].

Theoretical consideration for the $3S - 4S$ two-photon transition probability gives an analytical formula given as a function of the chirp rate and the pulse intensity, for

[3] Four-photon sequential path is 3S−4S − 7P 2 + 1 photon process in addition to 7P−4S one-photon de-excitation. In this experiment, several order of magnitude is smaller than two-photon direct path.

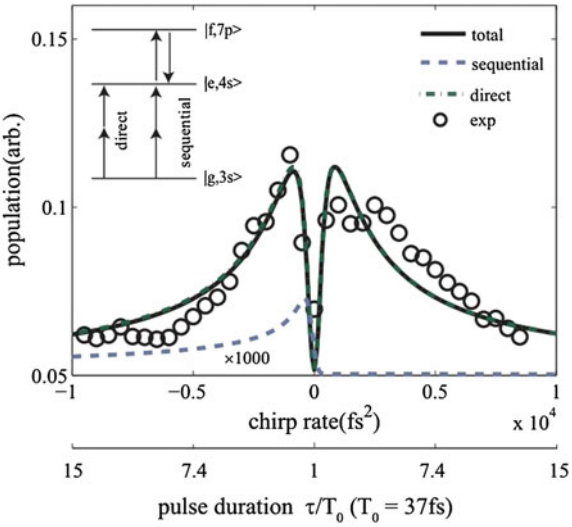

Fig. 4.9 Sodium two-photon absorption rate measured as a function of the chirp rate. The two-photon direct transition path turns out much larger than the four photon sequential transition path. The image is from [7] with permission by the publisher

the case of a zero de-tuning from the two-photon resonant condition, by

$$P_e \propto \frac{1}{\sqrt{1+4a_2^2/\tau_0^4}} \exp[-\frac{\pi\eta^2 I_0^2 \tau_0^2}{8(1+4a_2^2/\tau_0^4)}], \tag{4.8}$$

where a_2, τ_0, and I_0 are the chirp rate,[4] transform-limited pulse width (intensity) defined by $\exp(-t^2/\tau_0^2)$, and the peak intensity respectively. η in the equation has complicated physical origin, thus we just treat it as a fitting constant here.[5] Experimental result obtained as a function of the chirp rate and the pulse intensity is shown in Fig. 4.10. As the pulse intensity increases, a single peak centered at the zero chirp region becomes divided into double peaks with a sharp dip in the zero chirp, which behavior is similar to the case of Fig. 4.9. The exponential decay term in (4.8) properly describes such a behavior: As the pulse intensity is big enough so that the dynamic Stark shift plays a role, the signal given as a function of the chirp rate appears with a dip point around the zero chirp with a symmetric double side peaks as shown in Fig. 4.10b. However, when the pulse intensity is low, the signal shows a usual behavior of a single peak around the zero chirp, as shown in Fig. 4.10c. The contour lines in Fig. 4.10 are theoretically calculated from (4.8).

[4] The linear spectral chirp Φ'' in (4.3) and a_2 here is identical parameter.

[5] For more detailed description, we would recommend readers to read [13].

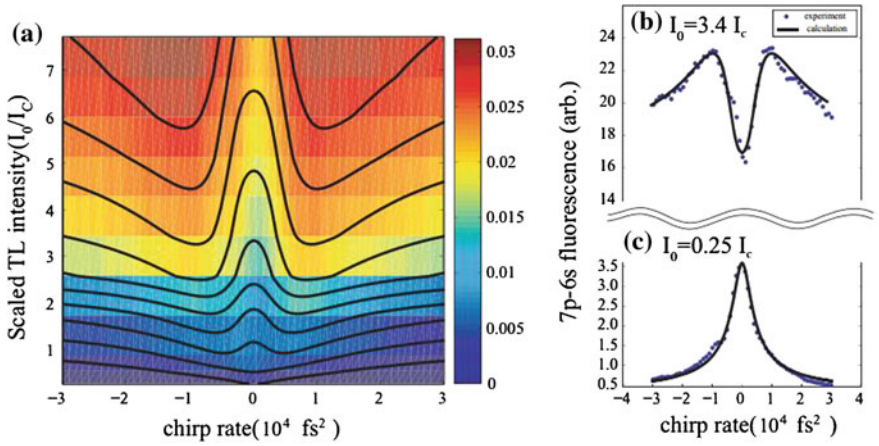

Fig. 4.10 **a** Two-photon transition probability to cesium 8 s state from the ground 6 s state measured as a function of chirp rate and pulse intensity. **b** and **c** show the behaviors in the strong and weak interaction regimes, respectively. The image is from [13] with permission by the publisher

So far, we have seen that the effect of dynamic Stark shift can decrease the two-photon transition in the strong field regime. The chirp rate, both negative and positive, could increase the transition rate by reducing the amount of energy level shift.

4.5.3 Optimal Pulse Shaping of a Two-Photon Transition

Then, one can also consider a case that a more sophisticated pulse shaping method could even compensate for the dynamic energy level shift to increase the transition [31]. The idea has been experimentally realized in the Cesium 6S–8S non-resonant two-photon transition case [32].

The cesium 6S–8S non-resonant two-photon transition can be described by a two-level system Hamiltonian [32],

$$H(t) = \hbar \begin{bmatrix} 0 & \frac{1}{2}\Omega(t)e^{2i\phi(t)} \\ \frac{1}{2}\Omega(t)e^{-2i\phi(t)} & \Delta + \delta(t) \end{bmatrix}, \tag{4.9}$$

by appying the unitary transformation $U(t) = |g><g| + e^{-2i\phi(t)}|e><e|$,

$$H(t) = \hbar \begin{bmatrix} 0 & \frac{1}{2}\Omega(t) \\ \frac{1}{2}\Omega(t) & \Delta + \delta(t) - 2\dot{\phi}(t) \end{bmatrix}, \tag{4.10}$$

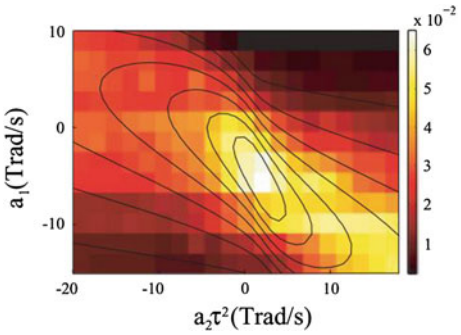

Fig. 4.11 Two-photon transition rate between the cesium 6S and 8S energy levels given as a function of the two control parameters a_1 and a_2 defined in (4.11). Measurements were carried out at the laser intensity of 0.21×10^{11} W/cm^2. The image is from [32] with permission by the publisher

where $\Omega(t)$ is the two-photon Rabi frequency and $\phi(t)$ is the phase of electric field. $\Delta = \omega_e - \omega_g - 2\omega_0$ is the de-tuning and $\delta(t)$ is the effective dynamic Stark shift. The $\delta(t)$ is proportional to intensity $I(t)$.

It is known that the population transfer by the Hamiltonian, (4.10) can be maximized by making the diagonal term of the Hamiltonian zero [31]. For this, the temporal pulse phase should satisfy the condition $2\dot{\phi}(t) = \Delta + \delta(t)$, or the system maintains dynamically the resonant condition. To compensate the dynamic Stark shift, $\delta(t)$, which is proportional to the temporal pulse intensity $\exp(-t^2/\tau^2)$, we expand $\delta(t)$ as a Taylor series up to second term. Then, the compensation condition is given by,

$$2\phi(t) = (\Delta + \delta(0))t - \frac{1}{3}\frac{\delta(0)}{\tau^2}t^3 = 2a_1 t + 2a_2 t^3 \tag{4.11}$$

The temporal phase is described by a polynomial form similar to the (4.3) of the spectral phase. The zeroth order and the second order terms of the temporal phase have the same physical origins, respectively, as those of spectral phase, which are carrier envelop phase and chirp rate, respectively. While, the first order term of temporal phase, on the other hand, is different from that of spectral phase. The former corresponds to a shift of the frequency envelope and the latter the time envelope. The third order term of the temporal phase is hardly described by the spectral phase components only, because it needs both controls of the spectral amplitude and phase at the same time.

The experimental result in Fig. 4.11 shows a good agreement with the calculation that is depicted by the black contour lines. The calculation is the numerical result of the time dependent shröedinger equation based on the Hamiltonian in (4.10). The approximation terms of the dynamic Stark shift $\delta(t)$ up to second order is used. The intensity are kept low enough to prevent loss through the ionization passage. The parameter a_1 shifts the two-photon energy of the laser pulse toward the shifted 8S energy level near the resonant condition, and a_2 bends the temporal frequency shape to have a more overlapped temporal region with the temporal shape of the dynamic Stark shift. Higher order terms neglected in (4.11) would better supplement the compensation if considered.

4.5.4 Chirps in a V-Type System

It is worth to mention the effects of chirps on the V-type two-photon transition [22]. The transition probability of (4.7) for the V-type two-photon transition can be simplified when the pulse envelope is assumed to be of a gaussian shape, and the spectral phase has a chirp (a_2) and a quadratic chirp (a_3) only. After a straightforward algebra, the given 2-photon transition can be written as

$$c_{ba}^{(2)} = i\frac{\tilde{\mu}_{ba}}{\hbar^2}[i\pi\tilde{\mathscr{E}}(\bar{\omega}) - \mathscr{P}\int_{\infty}^{\infty}\frac{\tilde{\mathscr{E}}(\omega)}{\bar{\omega}-\omega}d\omega], \tag{4.12}$$

where $\tilde{\mu}_{ba} = \mu_{ga}\mu_{bg}\exp[-\omega_{ba}^2/2\Delta\omega^2 + ia_3\omega_{ba}^3/24]$, $\bar{\omega} = (\omega_{ag}+\omega_{bg})/2$, and $\tilde{\mathscr{E}}(\omega) = |\tilde{E}(\omega)|^2\exp(i\omega_{ba}d\phi/d\omega)$ is the effective electric field. We just write down the one-photon de-excitation probability amplitude calculated by first order perturbation [22],

$$\begin{aligned} c_{ge}^{(1)} &= \frac{i\mu_{eg}E_0}{\hbar}\int_{-\infty}^{t}\exp(-\frac{t'^2}{\tau_c^2})\times\exp\{-i[(\omega_{eg}-\omega_0)t' - \alpha t'^2]\}dt' \\ &\underset{=}{F.T}\ \frac{\mu_{eg}}{\hbar}[i\pi\tilde{E}^*(\omega_{eg}) - \mathscr{P}\int_{-\infty}^{\infty}\frac{\tilde{E}^*(\omega)e^{i(\omega-\omega_{eg})t}}{\omega_{eg}-\omega}d\omega], \end{aligned} \tag{4.13}$$

where $\tau_c = \tau_0\sqrt{1+a_2^2/\tau_0^4}$, $\alpha = 2a_2/(\tau_0^4+4a_2^2)$, and τ_0 is the transform-limited pulse width (field) [22]. The readers should notice that the linear chirp rate is introduced in the de-excitation pulse for the case of (4.13). At time $t = 0$, (4.12) and the second (4.13) are of a similar form. Thus, the V-type two-photon transition process may be reduced to a one-photon de-excitation process. We conduct inverse Fourier transformation of (4.12) with an appropriate substitution of the effective electric field $\tilde{\mathscr{E}}(\omega)$ by a temporal shift $\tilde{t} = \omega_{ba}a_2$ and a chirp $\tilde{a}_2 = -\omega_{ba}a_3$. We can find its time domain form of (4.12) as

$$\begin{aligned} c_{ba}^{(2)} = &-\frac{\tilde{\mu}_{ba}E_0^2e^{i\theta}}{\hbar^2}\frac{\Delta\omega}{\sqrt{\tilde{\tau}_c/\tilde{\tau}_0}}\int_{-\infty}^{\tilde{t}}\exp(-\frac{t'^2}{\tilde{\tau}_c^2}) \\ &\times\exp\{-i[(\bar{\omega}-\omega_0)t' - \tilde{\alpha}t'^2]\}dt' \end{aligned} \tag{4.14}$$

where $\theta = -\frac{1}{2}\tan^{-1}2\tilde{a}_2/\tilde{\tau}_0^2 + (\bar{\omega}-\omega_0)\tilde{t}$, $\tilde{\tau}_0 = 2\sqrt{2}/\Delta\omega$, $\tilde{\tau}_c = \tilde{\tau}_0\sqrt{1+\tilde{a}_2^2/\tilde{\tau}_0^4}$, and $\tilde{\alpha} = 2\tilde{a}_2/(\tilde{\tau}_0^4+4\tilde{a}_2^2)$.

We note that the V-type two-photon transition probability amplitude in (4.7) is a result of infinite temporal integration, but the reduced probability amplitude in (4.14)

exhibits a time dependent-like form. The time dependence is in fact originated from the fact that the effective electric field is time-shifted proportional to the chirp rate, $\tilde{t} = \omega_{ba} a_2$. Interestingly, the V-type transition shows a coherent transient (CT)-like behavior as the chirp rate is controlled, although it should be distinguished from the real CT effect observed in pump-probe experiments [33–35].

Experimental result shown in Fig. 4.12I indeed exhibits the fore-mentioned CT-like behavior as a function of chirp rate. It is noted that three-pulse two-dimension Fourier transform spectroscopy can recover both the amplitude and phase of probability amplitude as shown in Fig. 4.12II.[6]

4.6 Spectral Phase Programming

One can also consider an arbitrary spectral phase function programming for the purpose of an optimized multi-photon transition. In particular, if the constituent transition pathways of the given transition are fully understood in terms of their respective phase information, maximally constructive quantum interference can be achieved by properly encoding the spectral phase function of the control laser pulse.

4.6.1 Spectral Phase Programming for a V-Type Transition

We consider the V-type two-photon system again, as an example. The target transition, between the adjacent fine structure energy levels through the ground state, is controlled by programming a spectral phase step at the spectral region $[\omega_{ag}, \omega_{ag} + \omega_{ba}]$. The governing equation is given in (4.7), where the integral term of (4.7) is decomposed into two part [21] as follows:

$$\begin{aligned} c_{ba}^{(2)} \simeq i \frac{\mu_{ga}\mu_{gb}}{\hbar^2} [& i\pi \tilde{E}^*(\omega_{ag}) \tilde{E}(\omega_{bg}) \\ & - e^{i\phi_b} \int_{\omega_{ag}-\omega_{ba}}^{\omega_{ag}} \frac{\tilde{E}^*(\omega)\tilde{E}(\omega_{ba}+\omega)}{|\omega_{ag}-\omega|} d\omega \\ & + e^{-i\phi_b} \int_{\omega_{ag}}^{\omega_{ag}+\omega_{ba}} \frac{\tilde{E}^*(\omega)\tilde{E}(\omega_{ba}+\omega)}{|\omega_{ag}-\omega|} d\omega], \end{aligned} \tag{4.15}$$

[6] Three ultra-fast pulses are incident on the target, with separately controllable pico-second scale time delays τ_1 and τ_2 between each consecutive pulse. The excited states induced by each pulse are interfered and the final fluorescence signal $I(\tau_1, \tau_2)$ is recorded. Two-dimensional Fourier transform of $I(\tau_1, \tau_2)$ acquires both amplitude and phase information. Detailed theoretical description on this experiment can be found from [22].

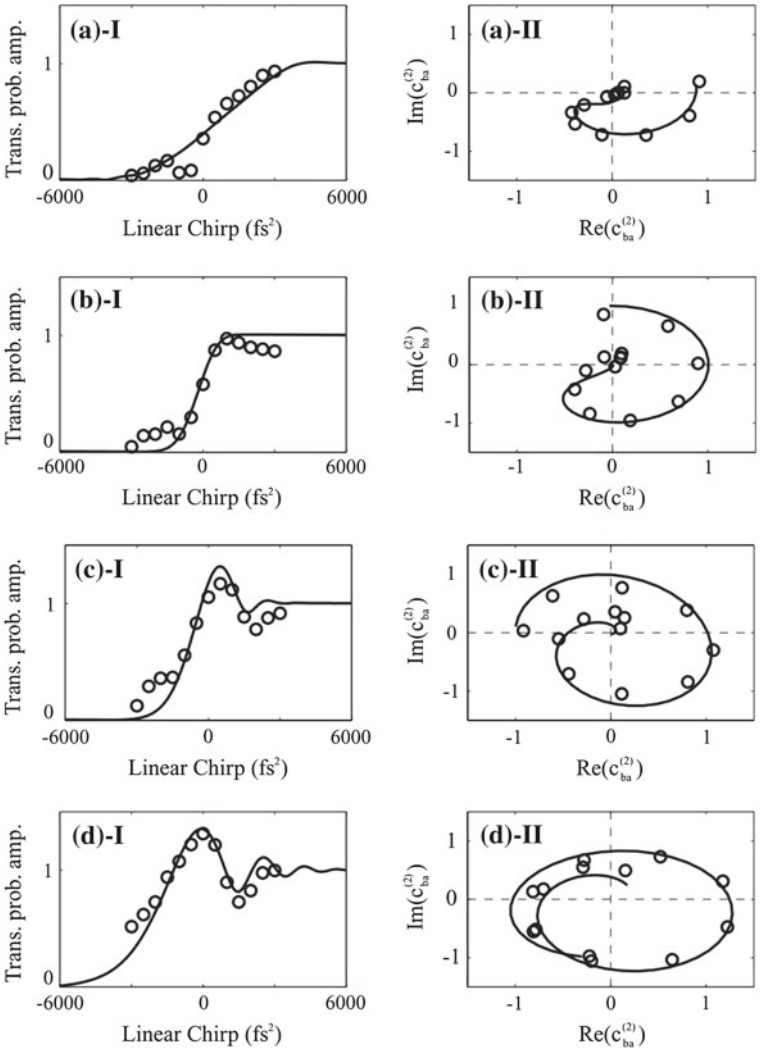

Fig. 4.12 Coherent transition-like behavior of the V-type two-photon transition as a function of linear chirp. The quadric chirps are given as **a** $-5 \times 10^4 fs^3$, **b** $-1 \times 10^4 fs^3$, **c** $3 \times 10^4 fs^3$, and **d** $7 \times 10^4 fs^3$. Sublabel **I** is the transition probability amplitude and **II** is the amplitude including the phase in complex plane. Solid lines are simulation and dots are experimental results. The image is from [22] with permission by the publisher

where the phase ϕ_b is the phase of the region $[\omega_{ag}, \omega_{ag} + \omega_{ba}]$, and the other regions have zero phase. The off-resonant components far from ω_{ag} are negligibly small thus omitted here.

The phase of the resonant part is fixed and the two non-resonant parts have rotating and counter-rotating phase, respectively. As the non-resonant components are

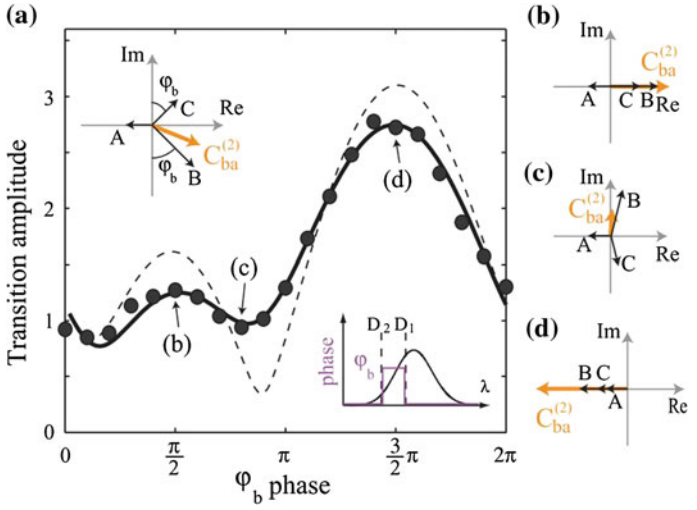

Fig. 4.13 **a** Transition amplitude with respect to the block spectral phase. Dots are experimental data, the *dashed line* is the simulation result based on (4.15), and the *solid line* is the simulation result with experimental systematic error. **b–d** Phase directions of each transition components of (4.15) with respect to the block spectral phase. The image is from [21] with permission by the publisher

initially, respectively, 90° out of phase from the resonant component, by manipulating the phase of the given spectral block, the transition amplitude shows an interference between the resonant and non-resonant components. The experimental and simulation results are shown in Fig. 4.13. The transition probability amplitude oscillates as the phase of the spectral block in $[\omega_{ag}, \omega_{ag} + \omega_{ba}]$ increases.

4.6.2 *Spectral Phase Programming for a Non-resonant Two-Photon Transition*

Another appreciable problem is the non-resonant two-photon transition [3]. As the non-resonant two-photon transition probability amplitude is written as a result of the second-order perturbation calculation as

$$c_{nr}^{(2)} \propto \int_{-\infty}^{\infty} |E(\omega_0/2+\omega)E(\omega_0/2-\omega)| e^{i[\phi(\omega_0/2+\omega)+\phi(\omega_0/2-\omega)]} d\omega, \qquad (4.16)$$

the transition has maximum when the spectral phase becomes antisymmetric ($\phi(\omega_0/2+\omega) = -\phi(\omega_0/2-\omega)$) or zero. However, it is more complicated when the spectral phase is symmetric. The transition probability can be zero or not. For the

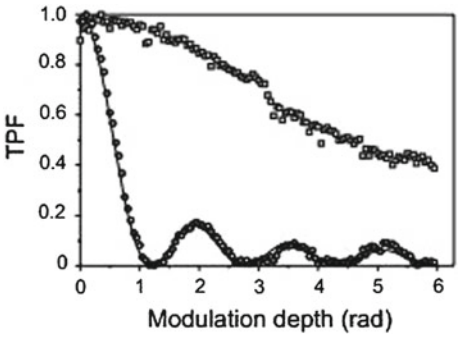

Fig. 4.14 Two-photon fluorescence with respect to modulation depth, A. The *Circle* and *square* data points are $C = 0$ and $C = \pi$ respectively. B is fixed at 220 fs. The image is from [3] with permission by the publisher

case of sinusoidal phase function, given by $A\cos(B\omega + C)$, the experiments has been performed with atomic cesium as in Fig. 4.14.

Then the two photon fluorescence signal measured as a function of the modulation depth A, for the cases of symmetric (circle) and antisymmetric (square) phase function. The antisymmetric sine phase predicts a flat, monotonic, two-photon transition, although it decays as the modulation depth grows. However, the result for a symmetric cosine phase shows much faster decay with periodic nodes, which behavior is well understood by the theoretical consideration in (4.14).

4.7 Conclusion

We have discussed various types of laser pulse shaping methods for coherent control of multi-level atomic systems. Spectral amplitude blocking in the ladder-type three-level two-photon transition in rubidium, and also in the V-type three-level two-photon transition in rubidium, has shown transition enhancements albeit the loss of pulse energy. Even in a simple two-level two-photon transition, coherent controls with spectral chirps have enhanced the transition in the strong field interaction case, due to the dynamic Stark shift, contradicting the common wisdom of nonlinear optics. Furthermore, the use of higher order chirps for the two-photon transition in a V-type three-level system has mimicked coherent transient-like behaviors. Ultimately, it has been found that optimal pulse shapes can be systematically designed by proper phase function programming for those transitions whose transition phase information is a priori known for all transition pathways. It is hoped that the pulse shaping method finds its versatile usage of ultra-short and ultra-broadband laser field not only for monitoring short time dynamics but also for surgically selective and diverse ways of quantum system controls.

References

1. C.J. Bardeen et al., Feedback quantum control of molecular electronic population transfer. Chem. Phys. Lett. **280**, 151–158 (1997)
2. A. Assion et al., Control of chemical reactions by feedback-optimized phase-shaped femtosecond laser pulses. Science **282**, 919–922 (1998)
3. D. Meshulach, Y. Silberberg, Coherent quantum control of two-photon transitions by a femtosecond laser puse. Nature **396**, 239–242 (1998)
4. G. Imeshev, M.A. Arbore, M.M. Fejer, A. Galvanauskas, M. Fermann, D. Harter, Ultrashort-pulse second-harmonic generation with longitudinally nonuniform quasi-phase-matching gratings: pulse compression and shaping. J. Opt. Soc. Am. B. **17**, 304–318 (2000)
5. S. Cialdi, M. Petrarca, C. Vicario, High-power third-harmonic flat pulse laser generation. Opt. Lett. **31**, 2885–2887 (2006)
6. N. Dudovich, B. Dayan, S.M. Gallagher-Faeder, Y. Silberberg, Transform-limited pulses are not optimal for resonant multiphoton transitions. Phys. Rev. Lett. **86**, 47–50 (2001)
7. S. Lee, J. Lim, C.Y. Park, J. Ahn, Strong-field quantum control of $2 + 1$ photon absorption of atomic sodium. Opt. Express **19**, 2266–2277 (2011)
8. B. Chang. Chen, S.H. Lim, Optimal laser pulse shaping for interferometric multiplex coherent anti-Stokes Raman scattering microscopy. J. Phys. Chem. B **112**, 3653–3661 (2008)
9. J.P. Ogilvie et al., Use of coherent control for selective two-photon fluorescence microscopy in live organisms. Opt. Express **14**, 759–766 (2006)
10. C. Rangan, P.H. Bucksbaum, Optimally shaped terahertz pulses for phase retrieval in a Rydberg-atom data register. Phys. Rev. A **64**, 033417 (2001)
11. B.E. Cole, J.B. Williams, B.T. King, M.S. Sherwin, C.R. Stanley, Coherent manipulation of semiconductor quantum bits with terahertz radiation. Nature **410**, 60–63 (2001)
12. W.S. Warren, H. Rabitz, M. Dahleh, Coherent control of quantum dynamics: the dream is alive. Science **259**, 1581–1589 (1993)
13. S. Lee, J. Lim, J. Ahn, Strong-field two-photon absorption in atomic cesium: an analytical control approach. Opt. Express **17**, 7648–7657 (2009)
14. A.M. Weiner, Femtosecond pulse shaping using spatial light modulators. Rev. Sci. Instrum. **71**, 1929 (2000)
15. A.M. Weiner, Ultrafast optical pulse shaping: a tutorial review. Opt. Comm. **284**, 3669–3692 (2011)
16. P. Tournois, Acousto-optic programmable dispersive filter for adaptive compensation of group delay time dispersion in laser systems. Opt. Comm. **140**, 245–249 (1997)
17. F. Verluise et al., Amplitude and phase control of ultrashort pulses by use of an acousto-optic programmable dispersive filter: pulse compression and shaping. Opt. Lett. **25**, 575–577 (2000)
18. T. Brixner, G. Gerber, Femtosecond polarization pulse shaping. Opt. Lett. **26**, 557–559 (2001)
19. J.C. Diels, W. Rudolph, *Ultrashort Laser Pulse Phenomena*, (Academic press, 1996), pp. 1–4
20. J. Lim, K. Lee, J. Ahn, Ultrafast Rabi flopping in a three-level energy ladder. Opt. Lett. **37**, 3378–3380 (2012)
21. J. Lim, H. Lee, S. Lee, J. Ahn, Quantum control in two-dimensional Fourier-transform spectroscopy. Phys. Rev. A. **84**, 013425 (2011)
22. J. Lim, H. Lee, J. Kim, S. Lee, J. Ahn, Coherent transients mimicked by two-photon coherent control of a three-level system. Phys. Rev. A. **83**, 053429 (2011)
23. A.M. Weiner, J.P. Heritage, E.M. Kirschner, High-resolution femtosecond pulse shaping. J. Opt. Soc. Am. B. **5**, 1563 (1988)
24. L. Xu et al., Programmable chirp compensation for 6-fs pulse generation with a prism-pair-formed pulse shaper. IEEE J. Quantum Electron. **36**, 893 (2000)
25. M.M. Wefers, K.A. Nelson, Programmable phase and amplitude femtosecond pulse shaping. Opt. Lett. **18**, 2032 (1993)
26. J.W. Wilson, P. Schlup, R.A. Bartels, Ultrafast phase and amplitude pulse shaping with a single, one-dimensional, high-resolution phase mask. Opt. Express. **15**, 8979 (2007)

27. A.M. Weiner, Femtosecond optical pulse shaping and processing. Prg. Quant. Electr. **19**, 161–237 (1995)
28. M.M. Wefers, K.A. Nelson, Analysis of programmable ultrashort waveform generation using liquid-crystal spatial light modulators. J. Opt. Soc. Am. B. **12**, 1343 (1995)
29. C. Tralleor-Herrero et al., Coherent control of strong field multiphoton absorption in the presence of dynamic Stark shifts. Phys. Rev. A. **71**, 013423 (2005)
30. B. Chatel, J. Degert, S. Stock, B. Girad, Competition between sequential and direct paths in a two-photon transition. Phys. Rev. A. **68**, 041402(R) (2003)
31. C. Trallero-Herrero, J.L. Cohen, T. Weinacht, Strong-field atomic phase matching. Phys. Rev. Lett. **96**, 063603 (2006)
32. S. Lee, J. Lim, J. Ahn, Strong-field two-photon transition by phase shaing. Phys. Rev. A. **82**, 023408 (2010)
33. S. Zamith, J. Degert, S. Stock, B.D. Beauvoir, Observation of coherent transients in ultrashort chirped excitation of an undamped two-level system. Phys. Rev. Lett. **87**, 033001 (2001)
34. J. Degert, W. Wohlleben, B. Chatel, M. Motzkus, B. Girad, Realization of a time-domain Fresnel lens with coherent control. Phys. Rev. Lett. **89**, 203003 (2002)
35. N. Dudovich, D. Oron, Y. Silberberg, Coherent transient enhancement of optically induced resonant transitions. Phys. Rev. Lett. **88**, 123004 (2002)